SLAC-PUB-913
(TH) and (EXP)
May 1971

PHOTOPRODUCTION OF MASSIVE MUON PAIRS AT HIGH ENERGIES*

Robert L. Jaffe†
Stanford Linear Accelerator Center, Stanford University, Stanford, California 94305

ABSTRACT

We study the high energy photoproduction of massive muon pairs off of protons in the framework of a field theoretical parton model. Parton annihilation is found to contribute to the production of high mass symmetric pairs. This contribution is important for events where a substantial fraction of the incident photon's momentum appears in the hadronic final state. It may be separated from the large background of Bethe-Heitler muon pairs by measuring a cross section differential in the muons' longitudinal momentum. We derive a scaling law for the parton annihilation contribution showing that the cross section measures the as yet unexplored structure function of the photon. Other mechanisms of muon pair production are discussed and shown to be negligible in the region where the parton effect is important. Finally we show that the parton contribution is observable despite the experimental complication of integrating the cross section over a bremsstrahlung photon spectrum.

(Submitted to Phys. Rev.)

---

* Supported in part by the U. S. Atomic Energy Commission.

† NSF Predoctoral Fellow.

INTRODUCTION

The parton model[1,2] is an attempt to explore in high energy physics the implications of a quasielastic or impulse approximation much like that of nuclear or atomic scattering[3]. Finding the reactions and kinematic regions in which the assumption of quasielasticity can be motivated has been a topic of considerable recent effort. Highly inelastic leptonic processes such as the Bjorken limit region of inelastic electron or neutrino scattering were the first to be discussed in a quasielastic approximation.[1,10]

In the past year the catalogue of highly inelastic leptonic processes has been extended to include production of very massive muon pairs in proton-nucleon collisions at very high energy as measured in the experimental work of Christenson et al.[4] Drell and Yan[5] have shown, in the framework of field theory with a transverse momentum cutoff, that the process $p + p \rightarrow (\mu^+\mu^-) +$ "anything" may be looked at in a parton model. There are, in addition, several other models for high energy, highly inelastic reactions[2], some of which have been applied to this process. Altarelli, Brandt and Preparata[6], and Sanda and Suzuki[7], have analysed the production of massive muon pairs in proton-nucleon collisions in terms of current commutators on the light cone and current algebra sum rules, respectively. Berman, Levy and Neff have investigated this process in perturbation theory.[8] Although, in principle, these approaches are sufficiently well defined to be distinguished experimentally present experimental data is not accurate enough to provide a test of the theories.

In this paper we investigate a process similar to that observed by Christenson et al.: the production of very massive muon pairs[9] by very high energy photons

incident on nucleons. Our objective is to examine whether this process can provide another arena for comparison of models of highly inelastic electrodynamic processes and, in particular, to investigate the parton structure of the photon. According to the parton model the real photon is some fraction of the time a bare photon and the rest of the time a superposition of parton anti-parton pairs. It is this parton structure of the real photon which we hope to study through an investigation of massive muon pair photoproduction.

Since the process $\gamma + p \rightarrow (\mu^+\mu^-) +$ "anything" is kinematically very similar to that investigated by Christenson et al. we expect the mechanism of parton pair annihilation (see Figure 1a) to emerge as dominant from our analysis much as it does from Drell and Yan's analysis[5] of the proton initiated process. There are, however, two substantial differences between the photon initiated reaction and the proton process. First, there is an experimental problem due to a large background of muon pairs from the Bethe-Heitler (BH) process illustrated in Figure 2. Indeed, the total cross-section for BH production of muon pairs dwarfs the parton contribution, however we find that there is a kinematic region in which the parton contribution may be seen above the BH background. Second, there is a theoretical difference in that the bare photon couples directly to each of the (charged) partons in the proton by means of what amounts to off mass-shell Compton scattering. This mechanism is illustrated in Figure 3. It has no analog in the proton initiated process. We show that in the limit of large dimuon mass and large incident photon energy and in the framework of the Drell-Levy-Yan (DLY)[10] model, the diagrams of Figure 3 admit a parton description; and, in fact, may be viewed as parton annihilation as in Figure 1a.

The result that a parton annihilation description of the Compton graphs of

Figure 3 is supported by the field theory model of DLY rests heavily on the large mass of the muon pair. In fact in this process the finite ratio of the dimuon mass Q^2 to the square of the total interaction energy, S, meets the requirements for applying a quasielastic approximation analogous to the Bjorken limit region in deep inelastic scattering. The same process but with the final muon pair having small mass was originally investigated in the parton model by Bjorken and Paschos[11], particularly for large momentum transfers. More recently, Brodsky and Roy[12] have shown that the field theory model of DLY does not support a parton picture for the production of low mass muon pairs except at very nearly forward angles. In the process of interest to us the large mass of the virtual photon which subsequently decays to the muon pair kinematically allows the virtual parton of Figure 3 to be nearly real. This is in contrast to the small photon mass case where the intermediate particle is highly virtual. The consequences of this difference will be discussed further in the following section.

In section II we derive a parton annihilation picture for the process $\gamma + p \rightarrow (\mu^+\mu^-) +$ "anything", paying particular attention to the Compton scattering of the bare photon as mentioned above. The cross-section for this process is found to be proportional to the product of the longitudinal momentum distributions at infinite momentum of the proton and photon. Since the proton's longitudinal momentum distribution is known from deep inelastic electron scattering, observation of this reaction measures the photon's distribution.

In Section III we calculate the BH background and establish the existence of a region in which the parton process predominates. In Section IV we mention other background processes and show that they should not be expected to contribute substantially in the same region as the parton process. Lastly we try to determine whether the process is experimentally observable in the kinematic region in which the parton mechanism predominates.

II. THE PARTON MECHANISM

A. General Considerations

The kinematics of muon pair creation are shown in Figure 4. We consider the limit in which the photon lab energy, $k = \frac{S}{2M_N} - \frac{M_N}{2}$ [13] and the dimuon mass, Q^2, are both much larger than any other mass in the problem. The ratio of Q^2 and S, $\tau = Q^2/S$ remains finite. We shall always be concerned with the symmetric kinematics in which case the muons have equal energies and make equal angles with the axis defined by the incident photon in the laboratory, i.e. $\epsilon_+ = \epsilon_-$ and $\theta_+ = \theta_-$.[14] The choice of symmetric kinematics is necessary, among other reasons, to remove interference terms between the BH and parton amplitudes.[15] Note, however, that we do not take the muons' momenta to be coplanar with the photon's, i.e. $\phi \neq \pi$. In terms of the variables $\Delta^\mu \equiv (p_+ - p_-)^\mu$ and $Q^\mu \equiv (p_+ + p_-)^\mu$ the symmetric case is defined by $\Delta_3 = 0$ and $\vec{\Delta}\cdot\vec{Q} = 0$. The 3-axis is taken along the direction of the incident photon.

In the large Q^2 and S limit and in a frame such as the center of mass where the momenta of both colliding particles are also very large, we assume both colliding particles to be comprised of a collection of approximately free constituents which Feynman has called partons[1], and which are assumed to be scattered quasi-elastically by the bare electromagnetic current[16]. These assumptions are supported by the work of DLY[10] who have established the parton model for highly inelastic electron scattering in a γ_5 field theory of pions and nucleons. The price one must pay for this description is the ad hoc introduction of a cutoff in the momentum transfer at hadronic vertices transverse to the infinite momentum direction. Alternatively, similar results may be obtained using a super-renormalizable theory such as ϕ^3. Such a cutoff is motivated by the observation that

the predominant interaction between colliding hadrons at very high energies carries only low momentum between them.

As mentioned in the previous section the model of DLY has been applied to the process $p + p \rightarrow (\mu^+\mu^-) +$ "anything" [5] with the result that the bremsstrahlung diagrams of Figure 1b are found to vanish, leaving only the parton annihilation graphs of Figure 1a to leading order. Exactly the same considerations apply to the photon induced reaction except for the existence of the additional diagrams of Figure 3 in which the bare photon Compton scatters (inelastically) off of a parton in the proton. Such diagrams do not occur in the DLY analysis of proton-proton process because Z_2, the amplitude for finding a bare proton in the physical proton, must be zero to account for the vanishing of the proton's electromagnetic form factor at large momentum transfer.[17]

Referring the reader to the analysis of reference 5, we assert that — except for the diagrams of Figure 3 — the photon initiated reaction also reduces to parton annihilation shown in Figure 1a in the large Q^2 and S limit. It is now necessary to prove the assertion made in Section I that the Compton graphs of Figure 3 also behave like parton annihilation in the large Q^2 and S limit and are therefore included in Figure 1a — and may therefore be treated as in reference 5.

B. Compton Graphs for Spin 0 Partons

In this section we compute the square of the covariant amplitude for the spin 0 parton Compton scattering diagrams of Figure 3a. We then show that the limit of this expression as Q^2 and S approach infinity is identical to the square of the time ordered Z-graph shown in Figure 5 in the same limit. Since the kinematics places the intermediate particle in Figure 5 approximately on energy shell and moving

along the direction of the incident photon, the figure represents the dissociation of the incident photon into a parton-antiparton pair and the subsequent annihilation of the antiparton on an incident parton in the proton. The covariant and gauge invariant amplitude for the three graphs of Figure 3a is:

$$M^{o}_{cov} = \left[\frac{1}{Q^2}\left\{2\lambda\left[j\cdot\epsilon - \frac{j\cdot k\epsilon\cdot Q}{k\cdot Q}\right] - \rho\left[\frac{j\cdot(2p'+Q)\epsilon\cdot(2p+k)}{(s-\mu^2)} + \frac{j\cdot(2p-Q)\epsilon\cdot(2p'-k)}{(u-\mu^2)} - 2\frac{j\cdot k\epsilon\cdot Q}{k\cdot Q}\right]\right\}\right]$$

$$\equiv M_{\mu\nu} j^{\mu} \epsilon^{\nu}$$

where $j^{\mu} \equiv \bar{u}(p_-)\gamma^{\mu}v(p_+)$, $s = (p+k)^2$ and $u = (p-Q)^2$.

The terms have been made individually gauge invariant and the parameters λ and ρ have been introduced to keep track of contribution of the seagull term. They will be set equal to unity later in the analysis. Squaring this, averaging over the polarizations of the initial photon and summing over the muon spins we obtain:

$$\tfrac{1}{2}\sum |M^{o}_{cov}|^2 = -\tfrac{1}{4} g^{\nu\tau}(\Delta^{\mu}\Delta^{\sigma} - Q^{\mu}Q^{\sigma} - Q^2 g^{\mu\sigma}) M_{\mu\nu} M_{\sigma\tau} \qquad (1)$$

The $Q^{\mu}Q^{\sigma}$ terms vanish by current conservation. To continue, we go the photon-proton center of mass frame. The transverse momentum cutoff of the DLY parton model limits the transverse momentum of the proton's constituents as S approaches infinity. We then assume that the parton has only limited transverse momentum: $p_{\perp} \leq M_N$. The restriction to symmetric muon pairs gives $\Delta\cdot k = 0$, also $\Delta\cdot Q = 0$ and $\Delta^2 = -Q^2$ (the muons are very relativistic), and from the $p_{\perp}$ restriction: $\Delta\cdot p = O(p_{\perp}\sqrt{Q^2})$. In the following calculation we take $Q_{\perp} = 0$ which implies $\Delta\cdot p' = O(p_{\perp}\sqrt{Q^2})$. This last restriction is for calculational convenience; later we shall see how the results we shall derive are dependent on the magnitude of $Q_{\perp}$. Eq. (1) reduces to

$$\tfrac{1}{2}\sum |\, M^{o}_{cov}\,|^2 = \frac{1}{4Q^2} \times$$

$$\left\{8\lambda^2 - 16\lambda\rho\left[1 + \frac{(Q^2-t)\mu^2}{(s-\mu^2)(u-\mu^2)} - \frac{Q^2}{Q^2-t}\right] + \rho^2\left[\frac{-16t}{Q^2-t} + \frac{4Q^2t + 16\mu^2Q^2 - 32\mu^2t}{(u-\mu^2)(s-\mu^2)} + \frac{4\mu^2(Q^2-t)^2(4\mu^2-Q^2)}{(u-\mu^2)^2(s-\mu^2)^2}\right]\right\} \tag{2}$$

$$+ \lambda^2/Q^2 + O(p_\perp^2)\ .$$

The term in curly brackets in Eq. (2) comes from the $g^{\mu\sigma}$ term of Eq. (1) while the remainder comes from the $\Delta^\mu\Delta^\sigma$ term of Eq. (1). To check Eq. (2) we set $Q^2 = 0$ and $j^\mu/Q^2 = \epsilon'^{\mu}$ and expect to obtain the usual spin 0 on-mass-shell Compton scattering formula. Comparison with Eq. (2) of reference 12 indicates that this is indeed the case.

Taking the large Q^2 and S limit of Eq. (2) we obtain:

$$\lim_{\substack{Q^2, S \to \infty \\ \tau \equiv Q^2/S \text{ fixed}}} \tfrac{1}{2}\sum |\, M^{o}_{cov}\,|^2 = \rho^2\left[\frac{tu - \mu^2Q^2}{s(u-\mu^2)^2}\right] \tag{3}$$

Essential in obtaining Eq. (3) is the observation that although Q^2, s and t approach infinity, u, which satisfies

$$u = 2\mu^2 + Q^2 - s - t \tag{4}$$

is of order $p_\perp^2$. Notice that the seagull terms do not contribute to Eq. (3) at all (we may now set $\rho = 1$). In the photon-proton center of mass, the center of mass momentum, $P \cong \sqrt{S}/2$, approaches infinity along with S. To leading order in S we may parametrize the momenta as follows:

$$\begin{aligned} k &= (P, \vec{0}, +P) \\ p &= \left(\eta P + (M^2 + p_\perp^2)/2\eta P, \vec{p}_\perp, -\eta P\right) \\ Q &= (Q_0, \vec{0}, Q_3)\ . \end{aligned} \tag{5}$$

For simplicity we leave the components transverse to the initial momentum as a 2-dimensional vector. In Eq. (5) η is the fraction of the proton's longitudinal momentum on the parton which is scattered. Using Eq. (4) to determine η, we obtain:

$$\eta = y_1 + \frac{(\mu^2 + p_\perp^2)}{4P^2}\left(\frac{y_1 + y_2 - 1}{y_2(1-y_1)}\right) \tag{6}$$

where $y_1 \equiv (Q_0 + Q_3)/2P$ and $y_2 \equiv (Q_0 - Q_3)/2P$ are a convenient pair of variables for much of our analysis. They are constrained by the kinematics as follows:

$$\tau \leq y_i \leq 1 \qquad \text{for } i = 1,2 \tag{7}$$

where $\tau \equiv Q^2/S$ is finite in our limit. In terms of the y-variables:

$$\begin{aligned} s &= y_2 S \\ t &= Q^2 - y_2 S \\ u &= \mu^2 - \frac{(\mu^2 + p_\perp^2)}{1-y_1} \end{aligned} \tag{8}$$

we obtain

$$\lim_{\substack{Q^2, S \to \infty \\ \tau \text{ fixed}}} \tfrac{1}{2} \sum |M^0_{cov}|^2 = \frac{p_\perp^2 (1-y_1)^2}{(\mu^2 + p_\perp^2)^2} \tag{9}$$

We now compute, using old-fashioned perturbation theory, the squared matrix element for the Z-graph of Figure 5.

$$M^0_Z = \frac{(p-\tilde{p})\cdot j\,(\tilde{p}-p')\cdot \epsilon}{2\tilde{E}Q^2(\tilde{E} + E' - k)} \ . \tag{10}$$

As usual in old-fashioned perturbation theory energy is not conserved at vertices, consequently $\tilde{p}$ is an on-mass-shell four vector ($\tilde{p}^2 = \mu^2$). We choose a transverse gauge for the present calculation and evaluate Eq. (10) in the photon-proton center

of mass and in the S, $Q^2 \to \infty$ limit. Squaring M_Z^o, summing over spins and using the parametrization of Eqs. (5) we obtain

$$\tfrac{1}{2}\sum |\, M_Z^o \,|^2 \;=\; \frac{p_\perp^2 (1-y_1)^2}{(\mu^2 + p_\perp^2)^2} \tag{11}$$

in exact agreement with Eq. (9).

The essential feature of the Z graph is that its energy denominator goes as $1/P$ making it dominant over the other time ordered graphs (energy denominators $\sim P$). The contact term vanishes because of its small numerator. This situation does not change at all if the outgoing photon is given a transverse momentum, $Q_\perp$, which is small compared to P, the only alteration is that $p_\perp^2$ in Eqs. (9) and (11) is replaced by something like $(Q_\perp + p_\perp)^2$.

To make the correspondence to parton annihilation we note that the longitudinal momenta of p' and $\tilde{p}$ are $(1-y_1)P$ and $y_1 P$ respectively; that is, they travel along the incident photon's direction (see Eq. (7)). This fact together with the observation that $\tilde{p}$ is nearly on energy shall comprises the parton annihilation picture. At least for spin zero partons we may then ignore graphs such as Figure 3a since dissociation of the photon into a parton anti-parton pair is already included in Figure 1a.

C. Compton Graphs for Spin $\frac{1}{2}$ Partons

The calculation for spin $\frac{1}{2}$ partons is simplified considerably if we borrow one of the results of Bjorken and Paschos' [11] work. In the course of discussing

photoproduction of low mass muon pairs they have computed the squared covariant matrix element for the diagrams of Figure 3b in the parton's rest frame. Taking the limit of Eq. (1) of reference 11 as Q^2 and S become infinite and using the kinematic restrictions of the previous section we obtain:

$$\lim_{\substack{Q^2, S \to \infty \\ \tau \text{ fixed}}} \tfrac{1}{2}\sum | M^{\frac{1}{2}}_{cov} |^2 = \frac{s}{4Q^2}\left[2p\cdot Q - Q^2\right]^{-1}$$

This result applies only in frames in which $\epsilon \cdot p = 0$. The proton-photon center-of-mass frame will not satisfy this restriction unless we consider only partons having $p_\perp = 0$. The results derived with $p_\perp = 0$ certainly apply for $p_\perp \lesssim M_N$, since the addition of a small transverse momentum cannot change the relative dominance of diagrams. Using the parametrization of momenta given in Eq. (5) and (6) and setting $p_\perp = 0$ we obtain:

$$\lim_{\substack{Q^2, S \to \infty \\ \tau \text{ fixed}}} \tfrac{1}{2}\sum | M^{\frac{1}{2}}_{cov} |^2 = \frac{1-y_1}{\mu^2 y_1} \tag{12}$$

The matrix element for the Z graph if Figure 5 in the case of spin $\frac{1}{2}$ partons is given by

$$M^{\frac{1}{2}}_{z} = \frac{\bar{u}(p')\not{\epsilon}(\not{\tilde{p}} - \mu)\not{j}u(p)}{2\tilde{E}(\tilde{E} + E' - k)Q^2}$$

Here again, $\tilde{p}$ is on mass shell, $\tilde{p}^2 = \mu^2$. Evaluating this in the photon-proton center-of-mass as S and Q^2 approach infinity, squaring and summing over spins and polarizations one obtains Eq. (12). We conclude, therefore, that the parton annihilation picture is valid for spin $\frac{1}{2}$ as well as spin 0 partons.

D. Calculation of the Differential Cross Section for Parton Annihilation

We have established that parton annihilation is the dominant parton process in the large S and Q^2 limit. It is now necessary to construct a differential cross section for this process for comparoson with the BH cross section. The cross section is computed in the usual manner.

$$d\sigma = (4\pi\alpha)^2 \frac{d^3p_+ d^3p_-}{\epsilon_+\epsilon_-} \left\{ \left[\tfrac{1}{2} Q^\mu Q^\nu - \tfrac{1}{2}\Delta^\mu\Delta^\nu - \tfrac{1}{2}Q^2 g^{\mu\nu} \right] \frac{1}{Q^4} \int {}_{\text{in}}\!< Pk \mid J_\mu(x) J_\nu(0) \mid Pk >_{\text{in}} e^{-iQ\cdot x} d^4x \right\} \tag{13}$$

In the large S and Q^2 limit we may use the techniques of DLY[10] to undress the current operators by means of the U-matrix and to argue that $U(t)U^+(0) \approx 1$. The integral of Eq. (13) becomes:

$$\int < U(Pk) \mid j_\mu(x) j_\nu(0) \mid U(Pk) > e^{-iQ\cdot x} d^4x \, .$$

If Q^2 were not large this step would not have been possible; it is at this point that this process differs from that discussed by Bjorken and Paschos[11] and Brodsky and Roy[12]. We now make the assumption discussed at length by Drell and Yan[5] that the U-matrix develops the photon and proton independently. The matrix element is thereby reduced to a sum over all possible parton-antiparton annihilations. Restricting ourselves to symmetric kinematics ($\Delta_3 = \vec{Q}\cdot\vec{\Delta} = 0$, although $Q_\perp$ need not be zero) the cross section may easily be computed. The result is:

$$d\sigma = (4\pi\alpha)^2 \frac{d^3p_+ d^3p_-}{Q^4 \epsilon_+\epsilon_-} \sum_a \left(\phi_p^a(p_2) \phi_\gamma^{\bar{a}}(p_1) \mid \frac{\lambda_a^2 f_a Q^2}{16\pi^2} \delta^4(Q - p_1 - p_2) \mid \phi_p^a(p_2) \phi_\gamma^{\bar{a}}(p_1) \right)$$

where the sum over "a" includes all species of partons. λ_a is the charge on parton

species "a" and f_a is 2 for spin zero partons and 1 for spin $\frac{1}{2}$ partons. The functions ϕ are momentum space "wavefunctions"; $\phi_p^a(p_2)$ is the amplitude to find a parton of type "a" and momentum p_2 in the proton; $\phi_\gamma^{\bar{a}}(p_1)$ is likewise the amplitude for an antiparton of type "a" in the photon. In the photon-proton center-of-mass in the large S limit the annihilating partons have momenta

$$\begin{aligned} p_1 &= \left(x_1 P + \frac{\mu^2 + k_1^2}{2x_1 P}, \vec{k}_1, x_1 P \right) \\ p_2 &= \left(x_2 P + \frac{\mu^2 + k_2^2}{2x_2 P}, \vec{k}_2, -x_2 P \right) . \end{aligned} \tag{14}$$

We now change variables to Δ^μ and Q^μ using $d^3p_+ d^3p_- = \frac{1}{8} d^3\Delta d^3Q$ and project out the symmetric differential cross section:

$$\left. \frac{d\sigma_{\text{PARTON}}}{dQ^2 dQ_3 d\Delta_3 d\left(\frac{\vec{\Delta}_\perp \cdot \vec{Q}_\perp}{|\vec{\Delta}_\perp| \, |\vec{Q}_\perp|} \right)} \right|_{\substack{\Delta_3 = 0 \\ \vec{\Delta}\cdot\vec{Q} = 0}} \equiv \int \frac{d\sigma}{dQ_3} \, \delta(Q^2 - \Delta_\perp^2) \, \delta(\Delta_3) \, \delta\left(\frac{\vec{\Delta}_\perp \cdot \vec{Q}_\perp}{|\vec{\Delta}_\perp| \, |\vec{Q}_\perp|} \right) \tag{15}$$

For notational convenience we define:

$$\left(\frac{d\sigma_{\text{PARTON}}}{dQ^2 dQ_3} \right)_{\text{SYM}} \equiv \left. \frac{d\sigma_{\text{PARTON}}}{dQ^2 dQ_3 d\Delta_3 d\left(\frac{\vec{\Delta}_\perp \cdot \vec{Q}_\perp}{|\vec{\Delta}_\perp| \, |\vec{Q}_\perp|} \right)} \right|_{\substack{\Delta_3 = 0 \\ \vec{\Delta}\cdot\vec{Q} = 0}}$$

The reasons for keeping the cross section differential not only in the dimuon mass but also in the dimuon laboratory momentum along the incident photon's direction will become apparent when we investigate the BH background. Carrying out the integrals in Eq. (15) we obtain:

$$\left(\frac{d\sigma_{PARTON}}{dQ^2 dQ_3^{lab}}\right)_{SYM} =$$

$$\frac{\alpha^2}{Q_0^{lab\,2} Q^4} \sum_a \lambda_a^2 f_a \tau \frac{Q_0^{cm}}{P} < \phi_P^a(x_2)\phi_\gamma^{\bar{a}}(x_1) \mid \delta\left(\frac{Q_3^{cm}}{P} - x_1 + x_2\right)\delta(x_1 x_2 - \tau) \mid \phi_P^a(x_2)\phi_\gamma^{\bar{a}}(x_1) > . \tag{16}$$

The structure of Eq. (16) is quite simple. It is a point annihilation cross section multiplied by a matrix element which measures the probability of finding a parton and an antiparton whose longitudinal momenta sum to Q_3^{cm} and whose invariant mass is Q^2. Eq. (16) may be simplified further. First we solve the δ functions for x_1 and x_2: $x_1 = (Q_0 + Q_3)/2P$ and $x_2 = (Q_0 - Q_3)/2P$ (all in center-of-mass). So the variables y_1 and y_2 introduced earlier measure the momentum fractions of the annihilating partons: $x_1 \equiv y_1$, $x_2 \equiv y_2$. Since $\tau < y_i < 1$,

$$\int_0^1 dz_1 \int_0^1 dz_2\ \delta(x_1 - z_1)\,\delta(x_2 - z_2) = 1$$

we have

$$< \phi_P^a(x_2)\phi_\gamma^{\bar{a}}(x_1) \mid \delta\left(\frac{Q_3^{cm}}{P} - x_1 + x_2\right)\delta(x_1 x_2 - \tau) \mid \phi_P^a(x_2)\phi_\gamma^{\bar{a}}(x_1) > =$$

$$\int_0^1 dz_1 \int_0^1 dz_2\ \delta\left(\frac{Q_3^{cm}}{P} - z_1 - z_2\right)\delta(z_1 z_2 - \tau) < \phi_\gamma^{\bar{a}}(x_1) \mid \delta(x_1 - z_1) \mid \phi_\gamma^{\bar{a}}(x_1) > < \phi_P^a(x_2) \mid \delta(x_2 - z_2) \mid \phi_P^a(x_2) >$$

These matrix elements measure the longitudinal momentum distribution of the photon and proton respectively. In the case of the proton

$$z_2 \lambda_a^2 < \phi_P^a(x_2) \mid \delta(x_2 - z_2) \mid \phi_P^a(x_2) > = F_2^a(z_2)$$

where $F_2^a(z_2)$ is the Bjorken limit of the contribution of partons of species "a" to νW_2. The scaling variable z_2 corresponds to $Q^2/2M\nu$ in electron scattering so that $F_2^a(z_2)$

is defined for $0 < z_2 < 1$. The photon matrix element defines a similar function for the antiparton of species "a" in the photon:

$$z_1 \lambda_a^2 < \phi_\gamma^{\bar{a}}(x_1) \mid \delta(x_1 - z_1) \mid \phi_\gamma^{\bar{a}}(x_1) > \equiv G_2^{\bar{a}}(z_1) .$$

Then finally

$$\left(\frac{d\sigma_{PARTON}}{dQ^2 dQ_3}\right)_{SYM} = \frac{\alpha^2}{Q_0^2 Q^4} \sum_a \frac{f_a}{\lambda_a^2} F_2^a(y_1) G_2^{\bar{a}}(y_2) . \qquad (17)$$

All of the quantities in Eq. (17) are evaluated in the lab except y_1 and y_2 which are, of course, defined in the center-of-mass. As promised, this cross section measures $G_2^{\bar{a}}$ since F_2^a is known and f_a and λ_a are numbers of order unity. An order of magnitude estimate of this cross section is obtained by noting that it is identical to that for the proton-proton case except that the structure function of the photon rather than the proton appears. Since the photon's coupling to hadrons is roughly a factor of $\alpha \equiv e^2/4\pi$ weaker than the proton's, the cross section of Eq. (17) should be smaller than that measured by Christenson et al.[4] by approximately two orders of magnitude. A detailed discussion of the actual shape of the cross section of Eq. (17) is deferred until the BH background has been computed. We note, however, that the shape of the proton's structure function ($F_2(y) \to 0$ as $y \to 1$), and a similar assumption for the photon's structure function imply that $(d\sigma/dQ^2 dQ_3)_{SYM}$ for fixed Q^2 is peaked near $y_1 = y_2$. The point $y_1 = y_2$ occurs at $Q_3^{cm} = 0$. The parton process is therefore largest in the middle range of the laboratory longitudinal momentum distribution. This is of primary importance in finding a region in which the parton process is dominant relative to the BH contribution discussed in the following section.

III. THE BETHE-HEITLER PROCESS

The cross section for production of massive lepton pairs by means of the Bethe-Heitler process[18] has been studied in detail over the past decade. Originally the process was of interest as a test of quantum electrodynamics[19] since the amplitude should be completely determined by the results of electron (or in our case, muon) scattering experiments. Early work was limited to the "elastic" case in which the target hadron is scattered elastically by the virtual photon. Later the theoretical work was extended by Drell and Walecka[20] to the inelastic process in which a sum over all possible hadronic final states is performed. In this section the results of Drell and Walecka are used to derive the BH contribution to the cross section, $(d\sigma/dQ^2 dQ_3)_{SYM}$. Our starting point is the totally differential cross section in the laboratory frame: Eqs. (23) and (26) of reference 20. Changing variables from p_+ and p_- to Δ and Q and integrating as in Eq. (15) we obtain:

$$\left(\frac{d\sigma_{BH}}{dQ^2 dQ_3}\right)_{SYM} = \frac{\alpha^3 Q_3^2}{16\pi M k^3} \int_{\cos\theta_{min}}^{\cos\theta_{max}} \frac{d\cos\theta}{\cos^3\theta} \frac{W_{\mu\nu} M^{\mu\nu}}{x^2 t^2} \tag{18}$$

$W_{\mu\nu} M^{\mu\nu}$ is the square of the invariant matrix element which is discussed later. Both x and t may be expressed in terms of S, Q^2, Q_3 and θ, where θ is the (equal) polar angle made by each of the symmetric muons with respect to the incident photon. x, which is the fraction of the incident photon's energy on either muon:

$$\epsilon_+ = \epsilon_- \equiv kx \equiv \left(\frac{S-M_N^2}{2M_N}\right) x \quad ,$$

is given by

$$x = \frac{Q_3}{2k\cos\theta} \tag{19}$$

while

$$t \equiv q^2 = Q^2 - 8k^2 x \sin^2 \frac{\theta}{2} \leq 0 .$$

The mass of the muon has been equal to zero in these expressions.[21]

Before going on to give an expression for $W_{\mu\nu} M^{\mu\nu}$ and evaluate Eq. (18) explicitly, it is necessary to discuss the kinematics of the process more carefully. We have used Q^2, Q_3 and θ as a complete set of variables for the production of symmetric pairs. The more usual set is x, θ and ϕ, in terms of which we find:

$$Q^2 = 4k^2 x^2 \sin^2 \theta \sin^2 \frac{\phi}{2} \qquad Q_3 = 2kx \cos\theta \tag{20}$$

For fixed Q^2 and Q_3 the limits on the θ integration are determined as follows. As θ is decreased $\sin^2 \frac{\phi}{2}$ must increase to maintain Q^2 constant. The minimum value of θ occurs when $\phi = \pi$; i.e. when the muons and the incident photon are coplanar. Explicitly:

$$\tan \theta_{min} = \frac{\sqrt{Q^2}}{Q_3} .$$

If θ were then increased holding Q_3 constant and $\phi = \pi$, Q^2 would increase. In order that Q^2 remain constant as θ increases, the angle ϕ decreases from π.

As θ increases $|t|$ increases (i.e. t becomes more negative). However since $M_f^2 - M_N^2 - 2M_N q_0 = |t|$ we have the inequality $-2M_N q_0 \geq |t|$ where $q_0 = k(2x-1)$. This restriction cuts off the θ integration at

$$\cos\theta_{max} = \frac{Q_3 (M_N + k)}{\left(M_N k + \frac{Q^2}{2} + k Q_3 \right)} .$$

Note that the elastic contribution always appears at θ_{max} and more generally that increasing θ at fixed Q^2 and Q_3 decreases the mass of the final hadronic state.

Since $|t|$ increases with θ, low mass final states contribute at relatively higher momentum transfer than high mass final states. This effect, which helps to diminsh the BH cross section, is more pronounced at small Q_3 where $|t|$ is generally larger. The variation of $|t|$ and the final hadronic state mass with Q_3 and θ is displayed in Figure 6.

Since $W_{\mu\nu} M^{\mu\nu}$ contains a δ-function contribution for the elastic peak we are able to remove the elastic piece from the integral in Eq. (18) and write it as an additional term with $\theta = \theta_{max}$.

One of the primary reasons for studying the kinematics in detail is to investigate the "volcano" effect[22] associated with the BH process. The so-called volcano is a steep and narrow minimum in the BH cross section at the point of complete symmetry, $\epsilon_+ = \epsilon_-$, $\theta_+ = \theta_-$ and $\underline{\phi = \pi}$. This near singularity occurs in the "elastic" BH process only when the magnetic moment contribution to the amplitude vanishes, and is therefore only prominant near $t = 0$. For a detailed discussion see the work of Henry[22]. If we set $\phi = \pi$ then it follows $t \equiv (k-Q)^2 \equiv (S-2M^2)(y_1 - 1)y_2$. Therefore t is near zero only when y_2 is as small as possible, or equivalently, when Q_3 is very large. Furthermore as we have just noted, for fixed Q_3 and Q^2 the heaviest mass hadronic final state occurs when $\theta = \theta_{min}$, i. e. where $\phi = \pi$.

Although for each Q^2 and Q_3 the integral of Eq. (18) touches the complete symmetry point at its lower limit we expect no volcano for the following reasons: first, the region of interest to us is that in which the parton process is large. As mentioned at the end of the previous section, for fixed Q^2 and S the parton mechanism is large when Q_3 in the laboratory is intermediate in value (see Figure 9). The variable y_2 is not small in this region, nor therefore, is t. Since t is not small

we expect no volcano. Second, because the interaction is most inelastic at θ_{min} (i. e. the hadronic final state mass is largest) and because the magnetic excitation of high mass hadronic states need not vanish even at $t \cong 0$, we should not expect to observe a volcano even in the "forward" region in which Q_3 is large and t small. This expectation has been borne out in explicit calculation; we have evaluated the integrand in Eq. (18) at points about symmetry and find only smooth and minor variations. The absence of a volcano simplifies calculation considerably since the theoretical cross section need not be averaged about symmetry to accommodate the finite acceptances of experimental devices.

With these kinematic considerations in mind we proceed in evaluating Eq. (18). The square of the matrix element may be written as follows[20]:

$$W_{\mu\nu} M^{\mu\nu} = \frac{4M_N}{A^2} \left[\left\{ \frac{2Q^2 t}{k^4} + 2A^2 \right\} W_1(q_0, t) + \left\{ \frac{Q^2}{k^2} \left(B - \frac{t}{k^2} \right) - A^2 - 2AB - \frac{t}{k^2} \right\} W_2(q_0, t) \right] \qquad (21)$$

where $A \equiv 2x(1-\cos\theta)$ and $B \equiv 1-2x$. The functions $W_1(q_0, t)$ and $W_2(q_0, t)$ are the structure functions of inelastic electron scattering as defined, for example, in Ref. 3. The elastic contribution to Eq. (21) may be separated out by writing:

$$W_i = \left[W_i\right]_{\text{inelastic}} + \frac{\delta(E-E'-q^0)}{E'} \left[W_i\right]_{\text{elastic}} \qquad (22)$$

E' is the energy of the final nucleon for the elastic case. $\left[W_i\right]_{\text{inelastic}}$ is the usual structure function which goes to zero at the elastic limit. $\left[W_i\right]_{\text{elastic}}$ may be written in terms of the nucleon's form factors as follows:

$$\left[W_1\right]_{\text{elastic}} = |t| \left[\tfrac{1}{2} F_1(t) + M_N F_2(t) \right]^2$$

$$\left[W_2\right]_{\text{elastic}} = M_N^2 \left[F_1^2(t) + |t| F_2^2(t) \right]$$

where

$$G_E(t) \equiv F_1(t) + \frac{|t|}{2M_N} F_2(t)$$

$$G_M(t) \equiv F_1(t) + 2M_N F_2(t)$$

The form factors are normalized by: $F_1(0) = 1$ and $F_2(0) = \frac{\kappa}{2M}$. Finally Eq. (18) may be rewritten with the elastic contribution separated out:

$$\left(\frac{d\sigma_{BH}}{dQ^2 dQ_3}\right)_{SYM} = \frac{\alpha^3 Q_3^2}{16\pi M_N k^3} \int_{\cos\theta_{min}}^{\cos\theta_{max}} \frac{d\cos\theta}{\cos^3\theta} \cdot \frac{\left[W_{\mu\nu} M^{\mu\nu}\right]_{inelastic}}{x^2 t^2} \tag{23}$$

$$+ \frac{\alpha^3 \left[W_{\mu\nu} M^{\mu\nu}\right]_{elastic}}{4\pi M_N k t^2_{max} \cos\theta_{max} \left[\frac{2M_N k x_{max}}{\cos\theta_{max}} \left[1 + \frac{k}{M_N}\left(1-\cos\theta_{max}\right)\right] + 2k^2 x_{max}\right]} .$$

$\left[W_{\mu\nu} M^{\mu\nu}\right]_{inelastic}$ and $\left[W_{\mu\nu} M^{\mu\nu}\right]_{elastic}$ are, of course, the contributions to Eq. (21) with W_i replaced by $\left[W_i\right]_{inelastic}$ and $\left[W_i\right]_{elastic}$ respectively.

We have evaluated this cross-section numerically using the following parametrizations of the data: for W_1 and W_2 at low t and q_0 we have used the SLAC data[23] separated using $R \equiv \sigma_L/\sigma_T = 0.15$ throughout. For highly inelastic scattering $\left(M_f^2 \geq 4 \text{ GeV}^2 \text{ or } |t| \geq 10 \text{ GeV}^2\right)$ we have used a fit[24] to the data in the scaling variable of Bloom and Gilman[25] for R = 0.18 :

$$|q_0| W_2(t, q_0) = (1-1/\omega')^3 \left[0.64 + 1.909\,(1-1/\omega') - 2.344\,(1-1/\omega')^2\right] \tag{24}$$

where $\omega' = (2M_N q_0 - M_N^2)/t$. For the elastic form factors we have used a modified dipole fit to elastic scattering data.

The results of this calculation are shown in Figure 7 where the cross section $(d\sigma_{BH}/dQ^2dQ_3)_{SYM}$ is plotted versus Q_3 for several values of Q^2 and S. The most striking and the essential feature of these results is the very rapid decrease of the cross section as Q_3 decreases from its maximum value. This decrease occurs as the virtual photon is forced off mass shell, not only removing the $1/t^2$ enhancement derived from its propagator, but also forcing the large elastic contribution and low lying resonances to progressively higher momentum transfer where they are suppressed by rapidly decreasing form factors. This behavior is shown explicitly in Figure 8 for several regions of hadronic final state mass. There one sees that for a specific Q_3, the contribution from the largest mass hadronic state which is kinematically allowed is the most important. In addition one sees the importance of the elastic peak in producing the large cross section near $Q_{3\,max}$. As was noted in the previous section, the parton mechanism contributions most strongly in the middle range of laboratory longitudinal momentum. The decrease of the BH contribution as shown in Figure 7 is sufficiently rapid to permit the parton process to dominate near the latter's maximum. The possibility of observing this effect experimentally is examined in the following section.

IV. EXPERIMENTAL IMPLICATIONS AND DISCUSSION

Having shown that the parton model provides a mechanism for the photoproduction of high mass muon pairs of not-too-large longitudinal momentum and that the BH background is strongly suppressed in the kinematic region of interest we must now show by explicit calculation that the parton process is dominant in a kinematic region where it yields an appreciable counting rate. We make a

quantitative estimate of the parton contribution. This must be compared to a realistic estimate of the BH background. In addition we must take account of such experimental handicaps as the absence of monochromatic photon beams. Finally, we must show that muon pair production mechanisms other than parton annihilation and BH are negligible in the kinematic region of interest.

In order to obtain a numerical estimate of the parton contribution an estimate of the photon's structure function $G_2^{\bar{a}}$ is needed. As argued earlier in this paper one expects the photon's hadronic interaction to be of order α compared to hadrons such as the nucleon. For the purposes of estimation we take $G_2^{\bar{a}}(x)$ to be simply proportional to the proton's structure function $F_2^a(x)$.[26] Of course it would be the object of any experimental measurement of the process to determine the function $G_2^{\bar{a}}(x)$. Therefore, for the purpose of obtaining a numerical estimate of the parton contribution we have set:

$$G_2^{\bar{a}}(y) = \frac{e^2}{f^2_{\rho\pi\pi}} F_2^a(y)$$

in which $e^2/f^2_{\rho\pi\pi} = 0.0029$ is the $\gamma\rho$ coupling constant derived from the pion form factor. Actually one expects the photon-hadron coupling to be somewhat larger than this if for no other reason than the contributions from the ω and ϕ mesons. This number may then be viewed as a lower limit. Again for the sake of computation all partons are taken to have the same momentum distribution, F_2, and the factor f_a/λ_a^2 has been set equal to unity. The resulting expression for the cross section is particularly simple:

$$\left(\frac{d\sigma_{\text{PARTON}}}{dQ^2 dQ_3}\right)_{\text{SYM}} = \frac{4\pi\alpha^3}{f^2_{\rho\pi\pi} Q_0^2 Q^4} F_2(y_1) F_2(y_2) \qquad (25)$$

We have computed this cross section using the scaling function of Eq. (24) with $\omega' = 1/y_i$; $i = 1, 2$. The results of this calculation are shown in Figure 9 for several values of Q^2 and S. It is apparent (see Figure 10) that for fixed S the BH background is not important in the region in which the parton annihilation process is large.

Before discussing the existence of other mechanisms for muon pair photoproduction we must make a digression concerning the actual experimentally accessible values of Q^2 and S. We have presumed these to be larger than any other masses in the problem. Reference to Figure 9 or Eq. (25) indicates that the parton contribution falls off rapidly in Q^2. In order to have a reasonable counting rate we shall have to accept values for Q^2 somewhat below the asymptotic region. We find that $S = 12$ GeV^2 and $Q^2 = 1.5$ GeV^2 are reasonable experimental parameters. In the case of inelastic electron scattering, spacelike values of Q^2 as low as 1 GeV^2 already show scaling behavior.[27] It is possible that this is also true for timelike photons. In any case, the first question to be answered experimentally is whether or not there exists an effect above the BH process. At this stage it is reasonable to relax the assumptions of asymptotically large S and Q^2. If an effect is indeed observed one must be more careful about these parameters when going on to a detailed comparison of Eq. (25) with experiment.

With these values of Q^2 and S in mind we wish to ask whether there is any other mechanism for muon pair photoproduction which might compete with parton pair annihilation in the region where it is large. This is impossible to answer in any systematic way, however, we can make some general remarks.

Processes, such as photoproduction of a massive vector meson as shown in Figure 11, which are primarily diffractive should be very small. The reason for this lies in the reaction's large momentum transfer: for $S = 12\ GeV^2$, $Q^2 = 1.5\ GeV^2$ and $Q_3 = 1.5\ GeV$ (a point near the parton process maximum), $|t| \geq 3.6\ GeV^2$. Assuming that Q^2 is greater than the mass squared of the ϕ meson, this mechanism should be bounded by the experimental upper limit in the production amplitude for high mass vector mesons times the vector meson's small ($\sim 10^{-4}$) branching ratio to $\mu^+\mu^-$ pairs. Using the recent experimental results of the SLAC and Cornell groups[28] and a $|t|$ dependence of $e^{-4|t|}$ [29] we conclude that the contribution of diffractively produced vector mesons is several orders of magnitude below the parton maximum.

One might expect a contribution from a U-channel Regge exchange as shown in Figure 12. Such a process accounts for the observed backward peak in vector meson photoproduction[30] and might contribute to μ pair photoproduction for $U \approx 0$. As discussed in Section II, $u \equiv (p-Q)^2 \cong 0$ where p is the momentum of the parton (in the proton) which annihilates with a parton in the photon. $U \equiv (P-Q)^2$, however, is not small. For the values of S, Q^2 and Q_3 in the preceeding paragraph $|u| \geq 1.25\ GeV^2$. At this distance from the backward enhancement,[30] the vector meson photoproduction cross section is again several orders of magnitude below the parton maximum.

For a fixed incident photon energy the parton mechanism is large enough to be observed above the background of BH events. We have estimated the counting rate one obtains from currently operational momochromatic photon beams (e.g. tagged photons or SLAC's laser source) and find it unacceptably low. One is then forced to consider bremsstrahlung beams which are available at higher intensities.

The primary complication due to integrating over a photon energy spectrum for a fixed Q^2 is that the BH "forward" peak (i. e. at the largest Q_3 for a given S and Q^2) from low energy photons will be at the same value of Q_3 as the parton contribution from high energy photons and will overwhelm it. Performing a subtraction experiment, i. e. running at two different maximum photon energies and subtracting the cross sections, would involve the difference of two very large numbers, burying the parton contribution in statistical uncertainty. This may be avoided by systematically excluding elastic BH events.

The large forward peak in the BH cross section is exclusively due to events in which the proton is elastically scattered by the virtual photon of Figure 2. This is best seen in Figure 8. We may systematically exclude elastic BH events by insisting that the μ-pair be deserved in coincidence with at least one meson. Since the parton annihilation mechanism creates a large amount of hadronic debris we do not expect this restriction to substantially reduce the parton contribution. Given this reduction in the BH forward peak, a subtraction experiment may now be possible. Fortunately, for fixed Q^2, the parton process maximum occurs at a nearly constant Q_3 over a range of incident photon energies. As a result, integrating over a photon distribution of several GeV does not spread out the parton peak. To see the effect of removing the elastic BH contribution and performing a subtraction experiment we have averaged $\left(\frac{d\sigma_{BH}}{dQ^2 dQ_3}\right)_{SYM}$ (inelastic events only) and $\left(\frac{d\sigma_{PARTON}}{dQ^2 dQ_3}\right)_{SYM}$ over a dk/k photon spectrum ranging from 8 to 12 GeV. The resulting cross sections are shown in Figure 13. One sees the continuing presence of a contribution from the parton annihilation mechanism.

V. SUMMARY AND CONCLUSIONS

We have shown that parton pair annihilation provides a mechanism for an anomalous production of massive muon pairs by high energy incident photons. In order to separate this contribution from the BH background it is necessary to consider a cross section differential in the longitudinal momentum of the muon pair. To remove interference between the BH and parton processes one is restricted to symmetric kinematic regions.[15] Several steps in the derivations of Section II require that the actual muon events rather than the experimental acceptances be symmetric. The absence of a volcano in the BH cross section decreases the sensitivity of our results to small departures from exactly symmetric events.

In addition to predicting the existence of an effect beyond the BH process, the parton model also predicts a scaling behavior for the cross section as seen from Eq. (17). By scaling behavior we mean that the parton contribution depends on Q^2, Q_3 and S only through the point cross section factors times a function of the ratios y_1 and y_2. Moreover, the cross section depends strongly on the photon's distribution which has not previously been studied experimentally. By measuring both the photon's mass and its longitudinal momentum the arguments y_1 and y_2 are fixed. The photon's structure function may therefore be measured point by point. This is in contrast to the case in which only Q^2 is measured[5], where the cross section depends on a convolution integral over the two structure functions.

It is important to emphasize the requirements made on the cross section which we have calculated. In addition to being limited to symmetrically detected pairs and to being differential in Q^2 and Q_3 we have also required that $Q_\perp$ be integrated over. If $Q_\perp$ were not integrated, the cross section would be sensitive to the

(unknown) transverse momentum distribution of the proton and photon and would not necessarily scale. Since the transverse momenta of the partons is assumed to be limited the $Q_\perp$ integral need not extend to very large values but must include the region $| Q_\perp | \leq M_N$.

In conclusion, we have established that a parton model can be motivated for the photoproduction of massive muon pairs and that the effect it predicts is observable above the BH background. If this effect can in fact be measured experimentally two further predictions of the parton model can be explored. First, the parton contribution to muon pair photoproduction should scale as a function of y_1 and y_2. If scaling is observed, supporting the application of the parton model to this process, the cross section can be interpreted to measure the photon's structure function.

VI. ACKNOWLEDGEMENTS

The author would like to thank Professor Sidney Drell for suggesting this problem and for many valuable discussions. In addition we are particularly grateful to Dr. S. Brodsky for very helpful discussions and for a careful reading of the manuscript, and to Dr. B. Wiik for many conversations concerning the experimental aspects of this paper. Conversations with Dr. F. Close and C. H. Llewellyn Smith are also gratefully acknowledged.

FOOTNOTES AND REFERENCES

1. R. P. Feynman, unpublished and in Phys. Rev. Letters 23, 1415 (1969), and Proceedings of the Third High Energy Conference at Stony Brook (Gordon and Breach 1970); J. D. Bjorken, Proceedings of the 1967 International School of Physics at Varenna (Academic Press, New York and London, 1968); J. D. Bjorken and E. A. Paschos, Phys. Rev. 185, 1975 (1969).
2. For a review of the current state of the parton model and other models for highly inelastic processes see: C. H. Llewellyn Smith, Ref. TH.1188-CERN (July 1970).
3. S. D. Drell, "Inelastic Electron Scattering, Asymptotic Behavior and Sum Rules" in A. Zichichi, ed., Subnuclear Phenomena (Academic Press, London, 1970).
4. J. H. Christenson et al., Phys. Rev. Letters 25, 1523 (1970).
5. S. D. Drell and T. M. Yan, Phys. Rev. Letters 25, 316 (1970); S. D. Drell and T. M. Yan, SLAC-PUB-808, to be published in Annals of Physics.
6. G. Altarelli, R. A. Brandt and G. Preparata, Phys. Rev. Letters 26, 42 (1971).
7. A. E. Sauda and M. Suzuki, to be published.
8. S. M. Berman, D. J. Levy and T. L. Neff, Phys. Rev. Letters 23, 1363 (1969).
9. Our analysis applies equally to the production of e^+e^- pairs.
10. S. D. Drell, D. J. Levy and T. M. Yan, Phys. Rev. Letters 22, 744 (1969); Phys. Rev. 187, 2159 (1969); Phys. Rev. D1, 1035 (1970); Phys. Rev. D1, 1617 (1970). S. D. Drell and T. M. Yan, Phys. Rev. D1, 2402 (1970). See especially the third reference.
11. J. D. Bjorken and E. A. Paschos, Phys. Rev. D1, 1450 (1970).
12. S. J. Brodsky and P. Roy, to be published.

13. We assume S and Q^2 large only in dynamical calculations, all masses are retained in the kinematics.

14. For the definition of all kinematic variables see Table I. The notation is that of J. D. Bjorken and S. D. Drell, Relativistic Quantum Mechanics (McGraw-Hill, New York, 1964).

15. For the interference to vanish it is enough that the experimental acceptances for both muons be symmetric. It is not necessary to sit exactly at $\theta_+ = \theta_-$ and $\epsilon_+ = \epsilon_-$.

16. It should be noted that the center of mass is not a "true" infinite momentum frame[5], by which we mean that the momentum of the colliding particles cannot become infinite while all invariants (e.g. Q^2, S, t) are held fixed. We have checked that all of the results which we obtain using a center of mass frame are equally valid in a true infinite momentum frame.

17. In addition, the transverse momentum cutoff at hadronic vertices would eliminate diagrams involving coupling of the bare proton to partons in the other proton.

18. H. A. Bethe and W. Heitler, Proc. Roy. Soc. (London) A146, 83 (1934).

19. S. D. Drell, Annals of Physics (New York) 4, 75 (1958); J. D. Bjorken, S. D. Drell and S. C. Frautschi, Phys. Rev. 112, 1405 (1958). J. G. Ashbury et al., Phys. Rev. 161, 1344 (1967). R. B. Blumenthal et al., Phys. Rev. 144, 1199 (1966) and further references found there.

20. S. D. Drell and J. D. Walecka, Annals of Physics (New York) 28, 18 (1964).

21. In performing the detailed numerical calculations outlined in this section we have retained the muon mass in all expressions in which it might not have been negligible. In particular it was retained in the expression for $W_{\mu\nu} M^{\mu\nu}$

fearing that it might be important in the region of the "volcano" discussed later in this section. This proved not to be the case in our kinematic region: ignoring the muon mass changes our results by no more than a few percent. All of the expressions of this section are therefore given in the relativistic approximation $m_\mu = 0$.

22. G. R. Henry, Phys. Rev. 153, 1649 (1967).

23. E. D. Bloom et al., Report presented to the XVth Conference on High Energy Physics, Kiev (SLAC-PUB-796) and references discussed there. Also G. Miller, SLAC-REPORT-129.

24. SLAC-MIT Electron Scattering Collaboration, to be published. A similar fit for R = 0.15 has come to our attention (cf. G. Miller, SLAC-REPORT-129).

25. E. D. Bloom and F. J. Gilman, Phys. Rev. Letters 25, 1140 (1970).

26. There is good reason to expect the photon structure function to have similar behavior as the proton structure function near x = 0 and 1. For $x \to 0$, the Regge behavior of high energy photon cross sections may be accounted for by taking $F(x) \to$ constant.[1] As $x \to 1$, phase space arguments imply $F(x) \to 0$. Quark model considerations support an even larger estimate for the cross section than that obtained using the proton's structure function to describe the photon. This result follows from the assumption that the partons are in fact quarks and include "valence" quarks which carry the particle's SU(3) quantum numbers (e.g. ppn for the proton) and a "sea" of $q\bar{q}$ pairs. The process $p + p \to (\mu^+\mu^-)$ + "anything" can proceed only by annihilation of a "valence" quark in one proton on a "sea" antiquark in the other or by annihilation of a "sea" quark in one or a "sea" antiquark in the other. The photon, on the other hand, would contain antiquarks among the "valence"

quarks since in this model it has the quark structure of a ρ^0 meson. The process $\gamma + p \rightarrow (\mu^+\mu^-)$ + "anything" would therefore be enhanced by the possibility of a "valence" antiquark in the photon annihilating on a "valence" quark in the proton.

As estimate of this enhancement depends on the exact distribution of "valence" and "sea" quarks as a function of longitudinal momentum. In a simple model due to Bjorken[31] and Feynman[1] the enhancement is roughly a factor of three, but the result is highly model dependent.

27. F. J. Gilman in Proceedings of the IVth International Symposium on Electron and Photon Interations at High Energies. Also see Figure 17 of E. D. Bloom et al., reference 23.

28. F. Bulos et al., Phys. Rev. Letters 26, 149 (1971). H. Alvensleben et al., Phys. Rev. Letters 26, 273 (1971).

29. P. Joos, Ref. DESY-HERA 70-1 and references cited there.

30. D. Tompkins et al., Phys. Rev. Letters 23, 725 (1969).

31. J. D. Bjorken, Report presented to the International Conference on Duality and Symmetry in Hadron Physics, Tel-Aviv (April, 1971); SLAC-PUB-905.

TABLE I

Glossary of Symbols

k^μ, ϵ^μ	—	4 momentum and polarization of incident γ-ray
P^μ	—	4 momentum of incident proton
P'^μ	—	4 momentum of final hadron state
$p^{\pm\mu}$	=	$(\epsilon^\pm, \vec{p}^\pm)$ — 4 momentum of $\mu^\pm$.
Q^μ	=	$(p^+ + p^-)^\mu$
Δ^μ	=	$(p^+ - p^-)^\mu$
q^μ	=	$(P-P')^\mu$ — 4 momentum of virtual photon in BH process
p^μ	—	4 momentum of initial parton, $p^2 = \mu^2$
p'^μ	—	4 momentum of final parton
$\tilde{p}^\mu$	—	4 momentum of virtual parton
S	=	$(k + P)^2$
t	=	$(k-Q)^2$
s	=	$(p + k)^2$
u	=	$(p-Q)^2$
$\theta_\pm$	—	polar angle of $\mu^\pm$ with respect to $\vec{k}$ in laboratory
ϕ	—	axumithal angle of muons with respect to $\vec{k}$ in laboratory
x	=	$\epsilon^\pm/k$ for the symmetric case where $\epsilon^+ = \epsilon^-$
P	—	center of mass momentum of photon and proton
y_1	=	$(Q_0^{cm} + Q_3^{cm})/2P$
y_2	=	$(Q_0^{cm} - Q_3^{cm})/2P$
τ	=	Q^2/S
M_N	—	nuclear mass
M_f	—	mass of final hadronic state

FIGURE CAPTIONS

1. Parton model diagrams for: a. parton pair annihilation into a massive muon pair; b. parton bremsstrahlung of a massive muon pair. The particle incoming on the left should be interpreted as a photon or a proton depending on the context.

2. Feynman diagrams for Bethe-Heitler production of muon pairs.

3. Feynman diagrams for inelastic Compton production of muon pairs off of partons in the proton: a. spin zero parton; b. spin $\frac{1}{2}$ parton.

4. Kinematics of muon pair production.

5. Time ordered Z graph for Compton production of a massive muon pair off of a parton (spin zero or $\frac{1}{2}$). Of the graphs of Figure 3 only this survives in the $S, Q^2 \to \infty$ limit (Q^2/S fixed).

6. a. Kinematic limits on the angular integral of Eq. (18) as a function of Q_3 for $S = 12$ GeV^2, $Q^2 = 3$ GeV^2.

   b. Contour lines of fixed final hadronic mass-squared (M_f^2; solid lines) and invariant momentum transfer (t; dotted lines) as a function of Q_3 and θ for the kinematic region shown in Figure 6a.

   For fixed Q_3, the angluar integral of Eq. (18) ranges over M_f^2 and t as shown in this figure.

7. Symmetric Bethe-Heitler cross section $\left(\frac{d\sigma_{BH}}{dQ^2 dQ_3}\right)_{SYM}$ for muon pair photoproduction as a function of Q_3 for fixed S and Q^2: a. $S = 12$ GeV^2; b. $S = 15$ GeV^2.

8. Symmetric Bethe-Heitler cross section $\left(\frac{d\sigma_{BH}}{dQ^2 dQ_3}\right)_{SYM}$ for muon pair photoproduction and final hadronic states of specific mass. $S = 12$ GeV^2; $Q^2 = 3$ GeV^2. The sum of the curves of this figure give the lower curve of Figure 7a.

9. Symmetric cross section for parton annihilation mechanism of muon pair photoproduction $\left(\frac{d\sigma_{PARTON}}{dQ^2 dQ_3}\right)_{SYM}$, as a function of Q_3 for fixed S and Q^2; a. $S = 12\ GeV^2$; b. $S = 15\ GeV^2$.

10. A comparison of the symmetric muon pair photoproduction cross sections from the BH mechanism and from the parton annihilation mechanism: a. $S = 12\ GeV^2$, $Q^2 = 1.5\ GeV^2$; b. $S = 15\ GeV^2$, $Q^2 = 3\ GeV^2$.

11. Diffractive photoproduction of a massive vector meson and its subsequent decay into a muon pair. The dotted line represents exchange of a Regge trajectory.

12. U-channel baryon Regge trajectory exchange for backwards μ-pair photoproductions.

13. Symmetric muon pair photoproduction cross sections averaged over a bremsstrahlung photon spectrum from $S = 8\ GeV^2$ to $S = 12\ GeV^2$. The BH and parton contributions are shown separately.

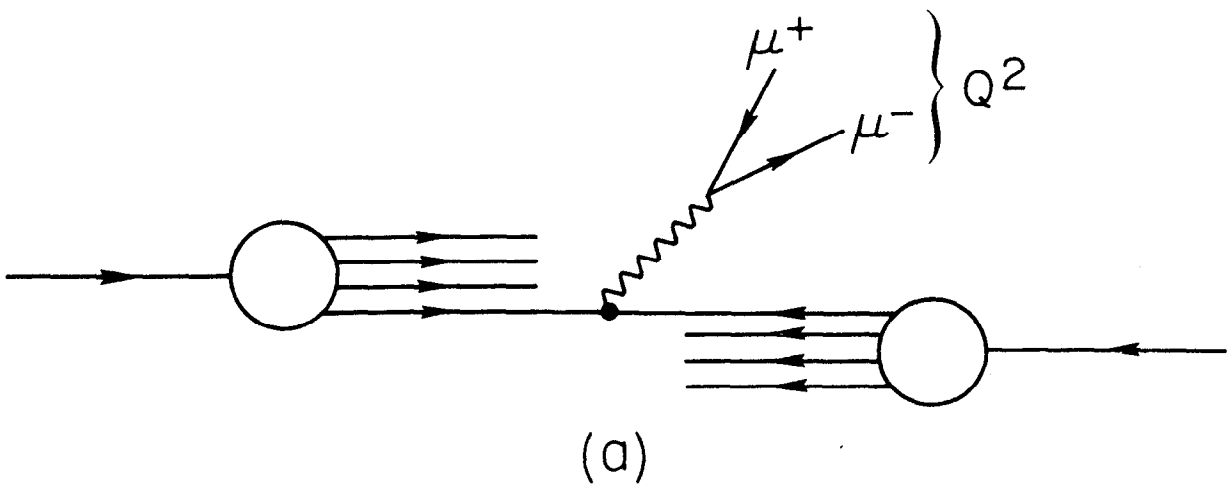

(a)

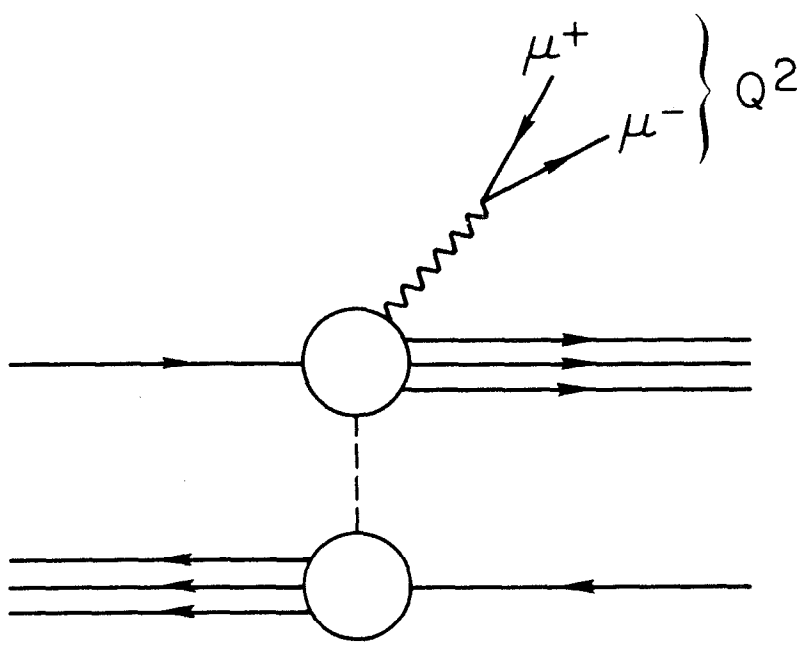

(b)

1873A1

Fig. 1

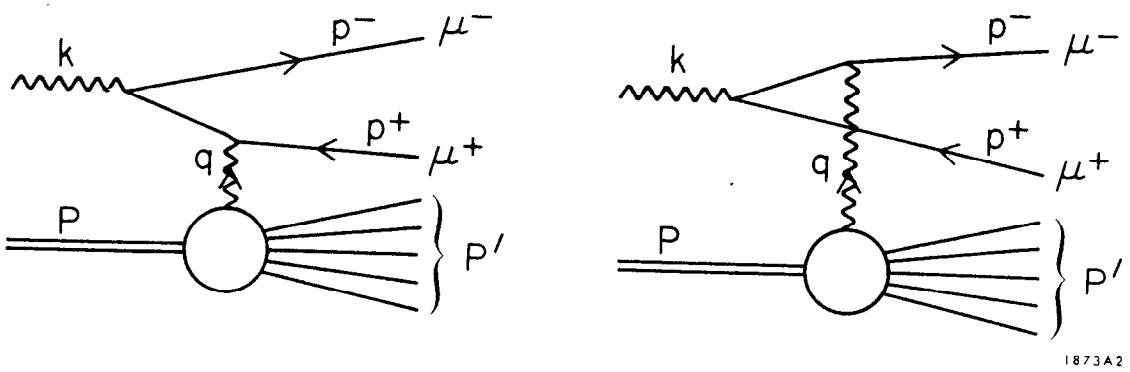

Fig. 2

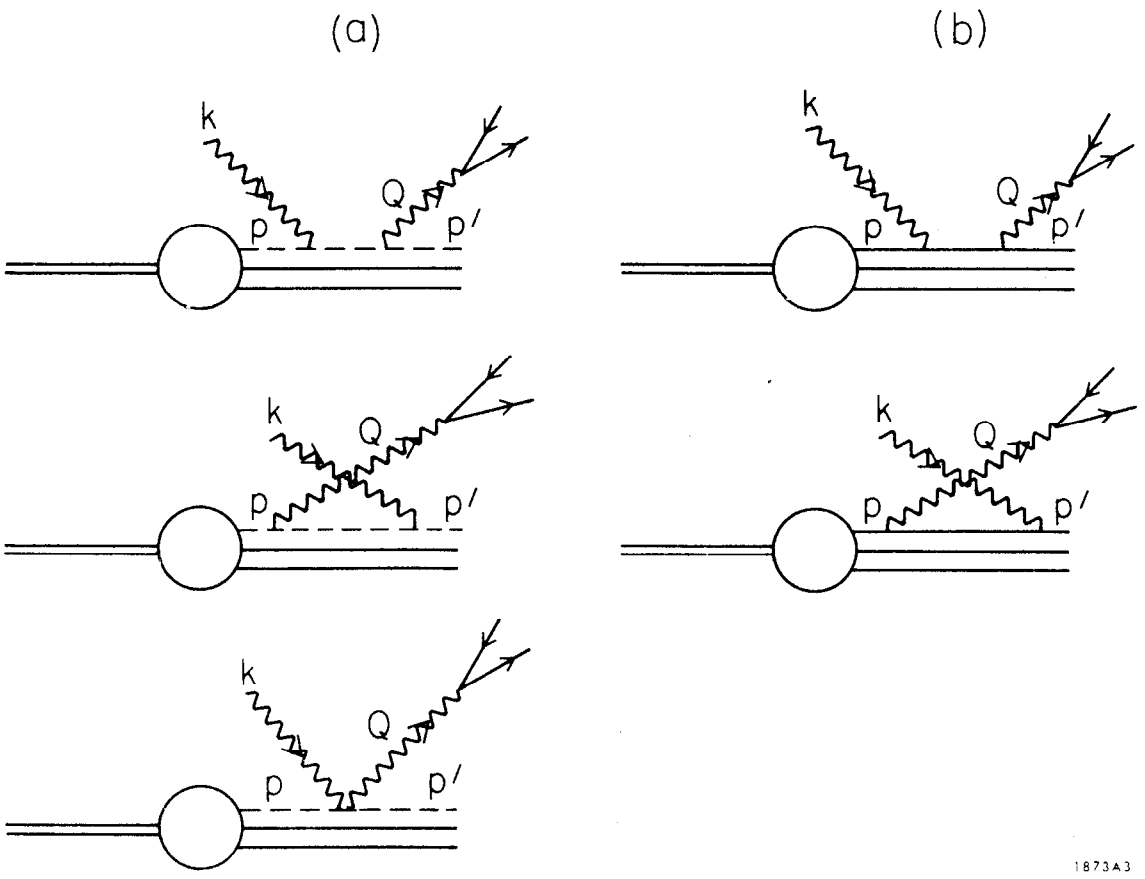

Fig. 3

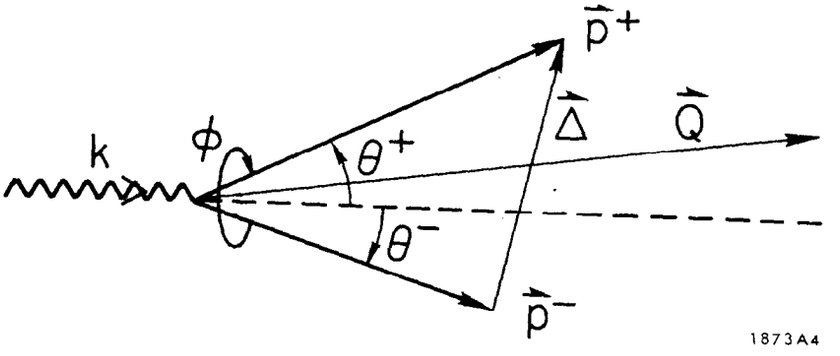

Fig. 4

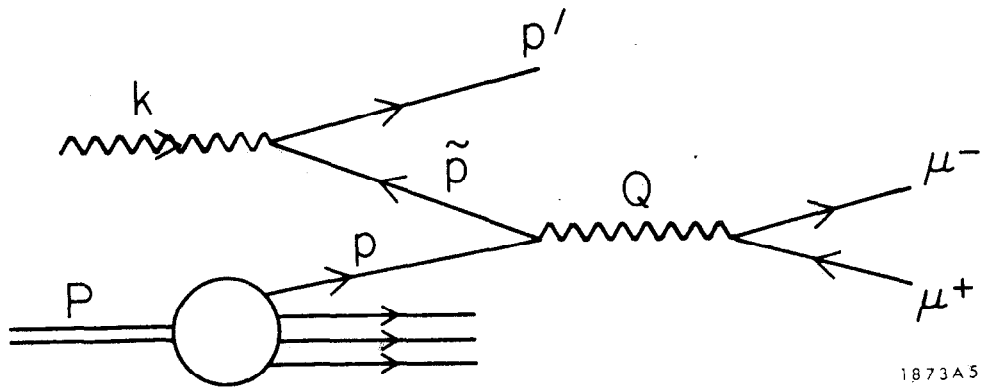

Fig. 5

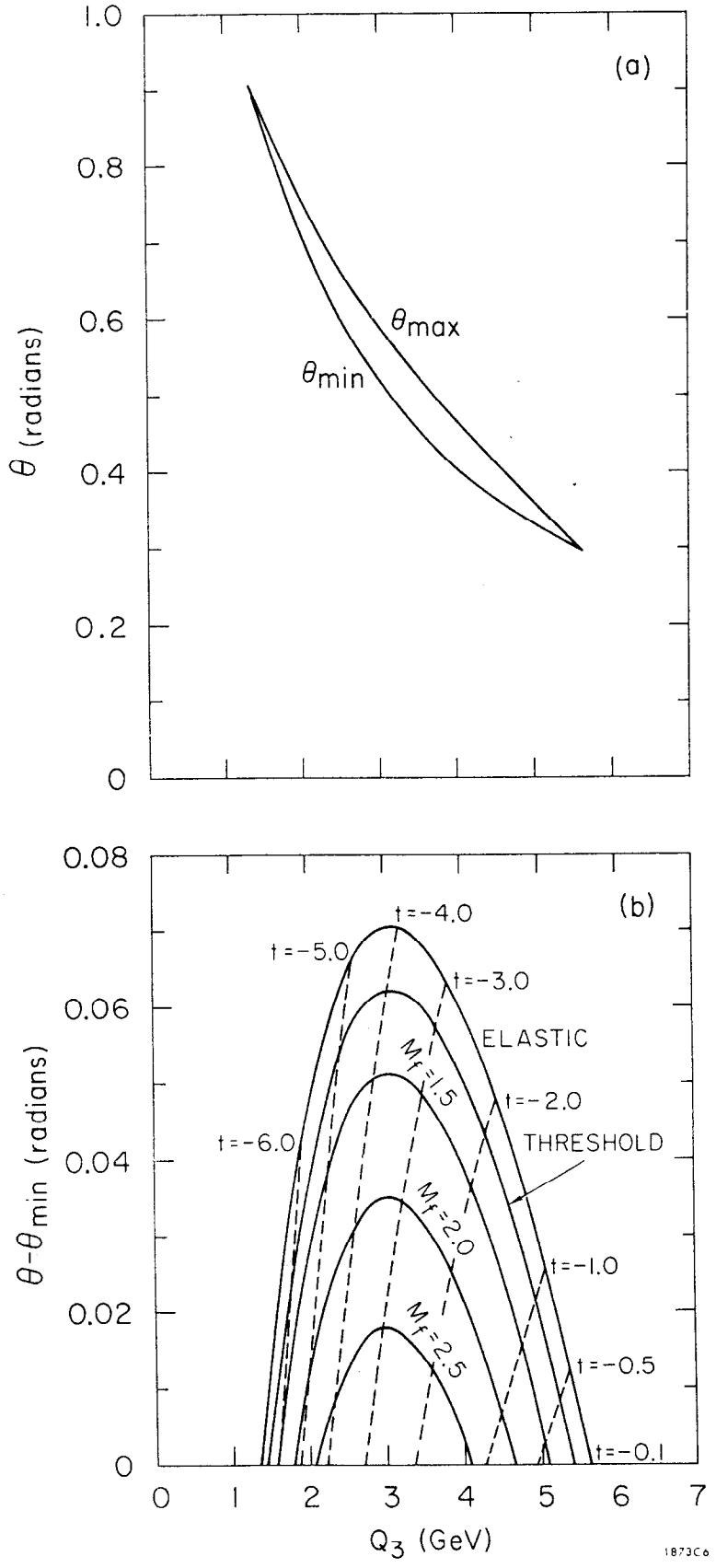
(a)
1.0
0.8
0.6
0.4
0.2
0
θ (radians)
θmax
θmin
(b)
0.08
0.06
0.04
0.02
0
θ-θmin (radians)
t=-4.0
t=-5.0
t=-3.0
ELASTIC
Mf=1.5
t=-2.0
t=-6.0
THRESHOLD
Mf=2.0
t=-1.0
Mf=2.5
t=-0.5
t=-0.1
0 1 2 3 4 5 6 7
Q3 (GeV)
1873C6

Fig. 6

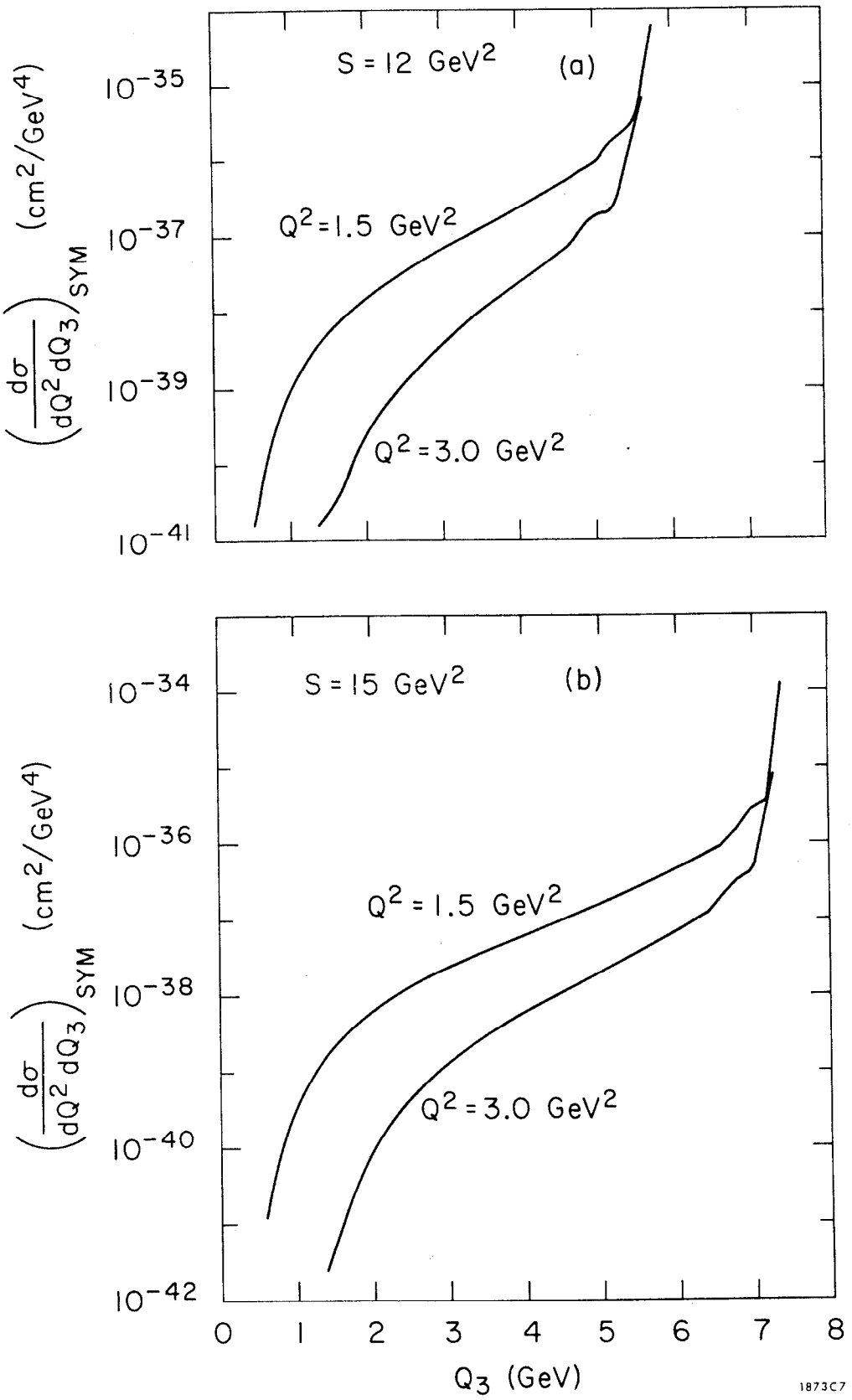
S = 12 GeV²
(a)
Q² = 1.5 GeV²
Q² = 3.0 GeV²
10⁻³⁵
10⁻³⁷
10⁻³⁹
10⁻⁴¹
(dσ/dQ² dQ₃)SYM (cm²/GeV⁴)
S = 15 GeV²
(b)
Q² = 1.5 GeV²
Q² = 3.0 GeV²
10⁻³⁴
10⁻³⁶
10⁻³⁸
10⁻⁴⁰
10⁻⁴²
0 1 2 3 4 5 6 7 8
Q₃ (GeV)
1873C7

Fig. 7

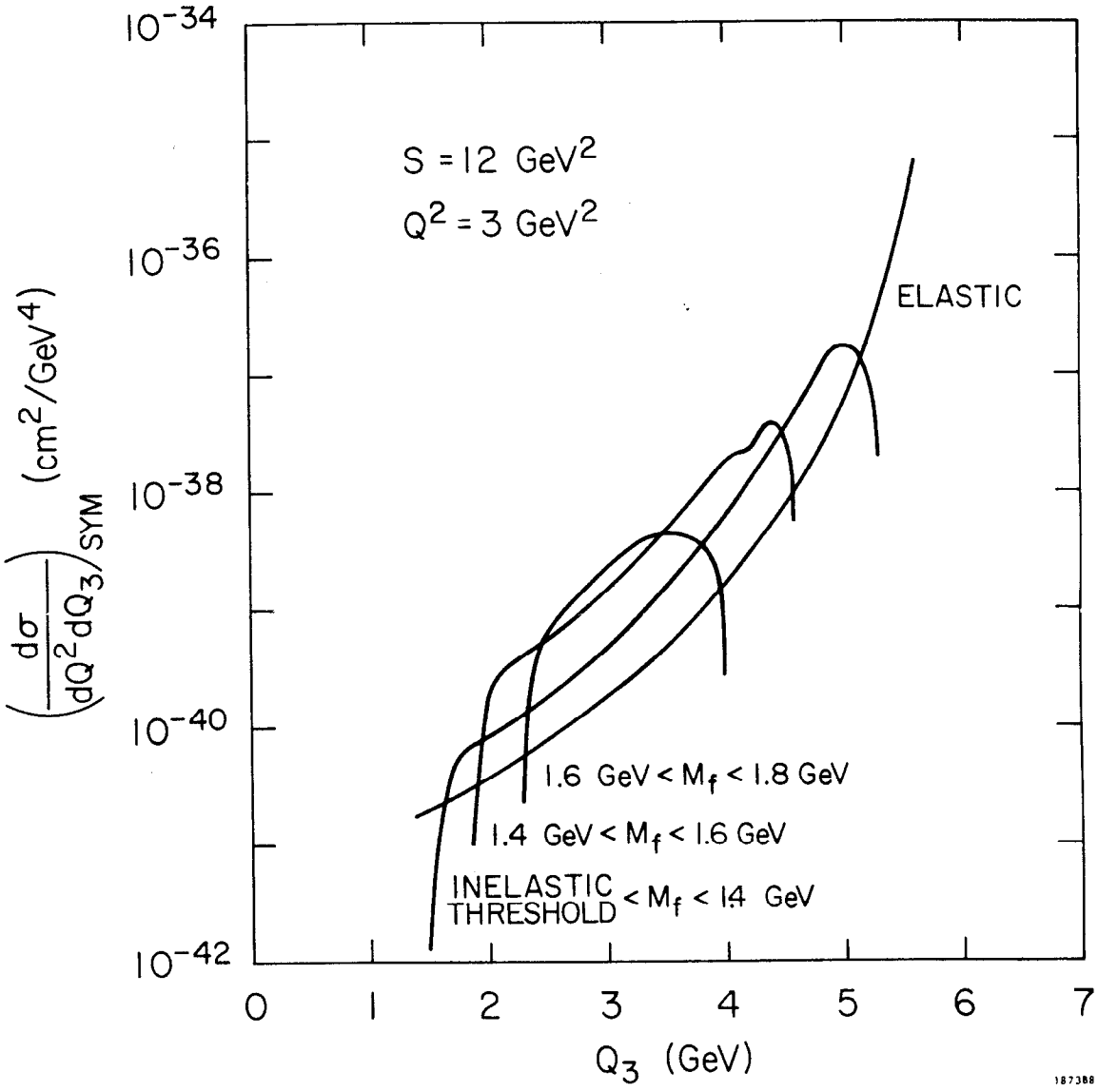
10^{-34}
10^{-36}
10^{-38}
10^{-40}
10^{-42}
$\left(\frac{d\sigma}{dQ^2 dQ_3}\right)_{SYM}$ (cm^2/GeV^4)
$S = 12\ GeV^2$
$Q^2 = 3\ GeV^2$
ELASTIC
$1.6\ GeV < M_f < 1.8\ GeV$
$1.4\ GeV < M_f < 1.6\ GeV$
INELASTIC THRESHOLD $< M_f < 1.4\ GeV$
0
1
2
3
4
5
6
7
Q_3 (GeV)
187388

Fig. 8

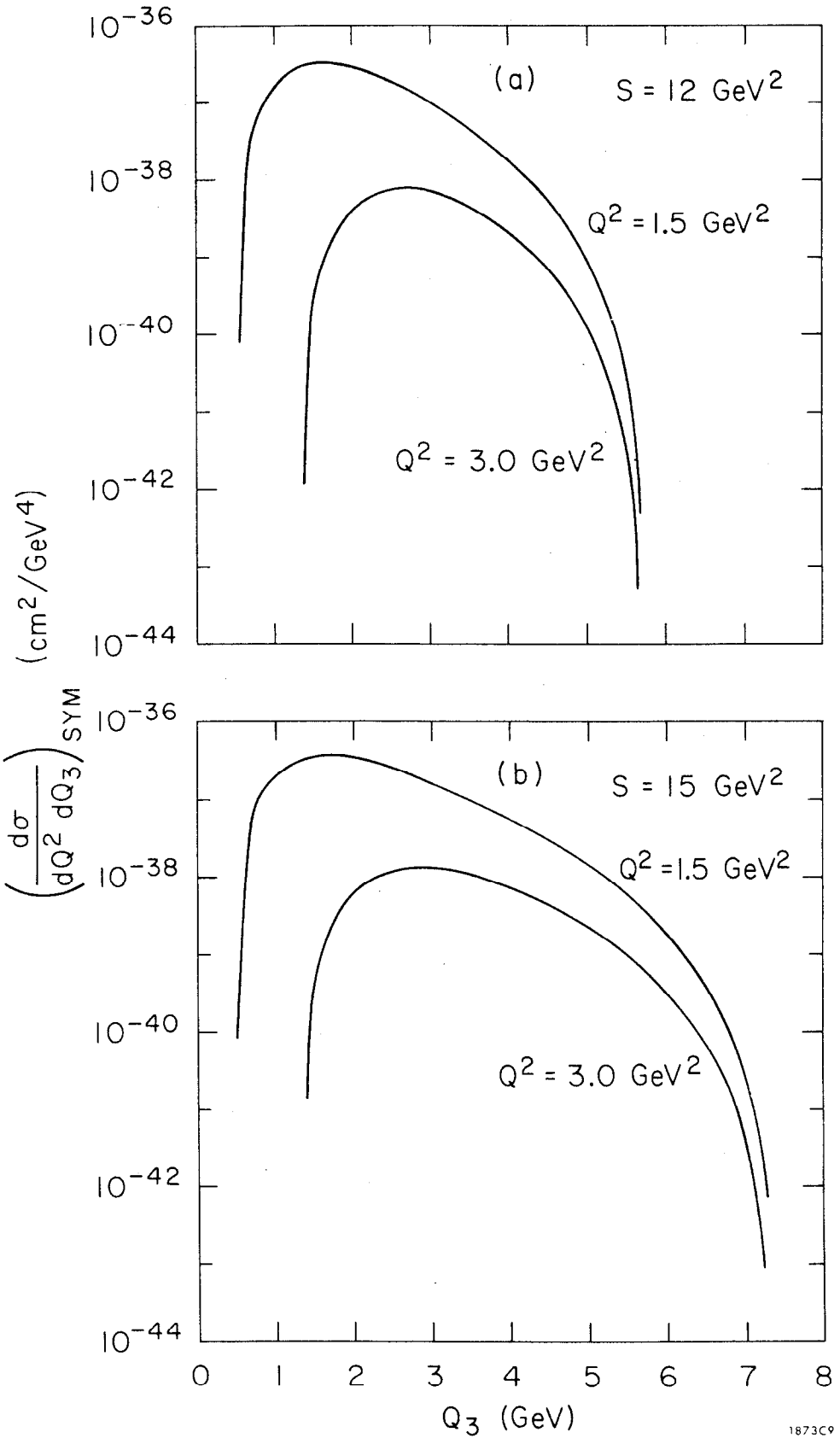
(a)
S = 12 GeV²
Q² = 1.5 GeV²
Q² = 3.0 GeV²
(b)
S = 15 GeV²
Q² = 1.5 GeV²
Q² = 3.0 GeV²
10⁻³⁶
10⁻³⁸
10⁻⁴⁰
10⁻⁴²
10⁻⁴⁴
(cm²/GeV⁴)
(dσ/dQ² dQ₃)SYM
0 1 2 3 4 5 6 7 8
Q₃ (GeV)
1873C9

Fig. 9

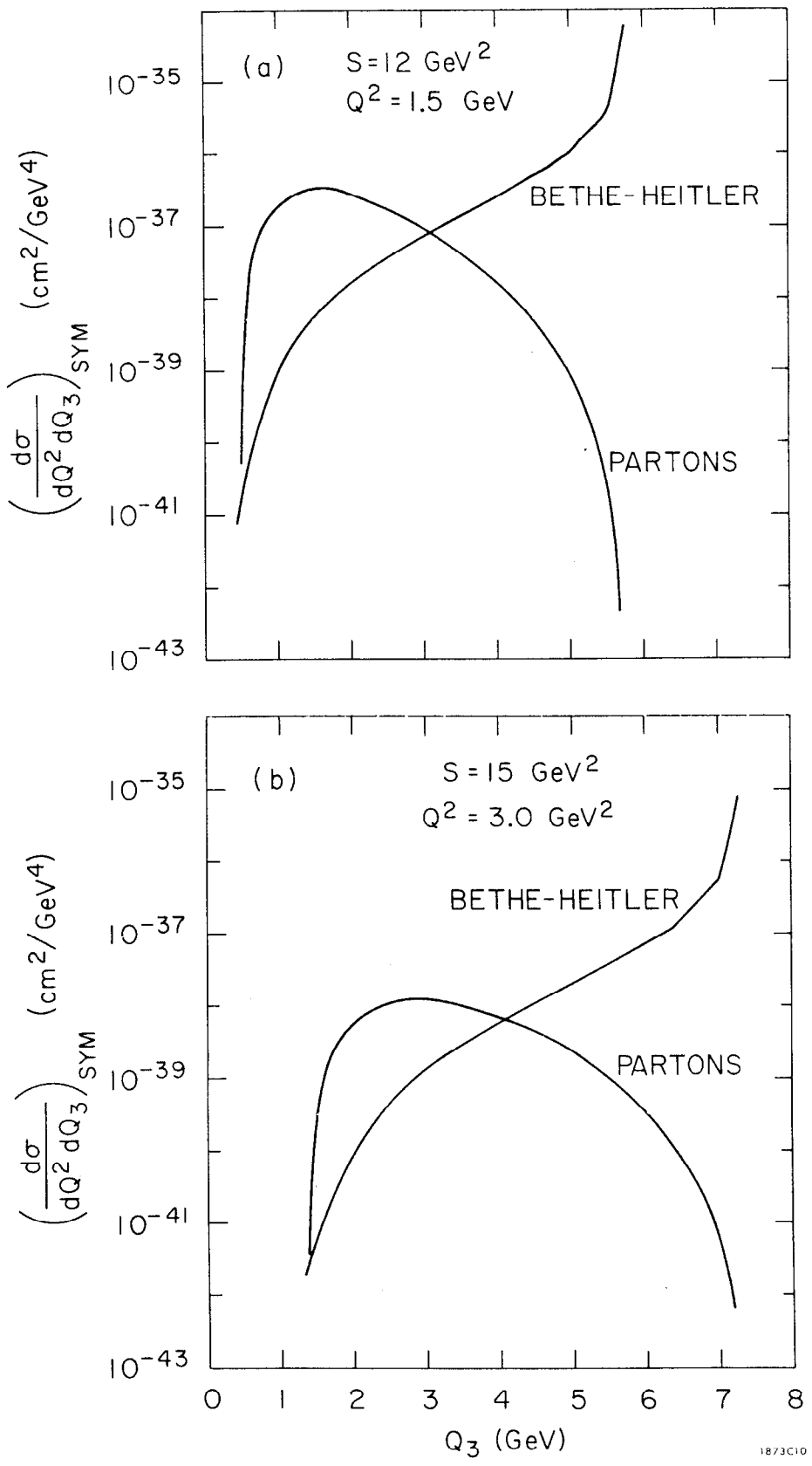
(a)
S = 12 GeV²
Q² = 1.5 GeV
BETHE-HEITLER
PARTONS
(b)
S = 15 GeV²
Q² = 3.0 GeV²
BETHE-HEITLER
PARTONS
10⁻³⁵
10⁻³⁷
10⁻³⁹
10⁻⁴¹
10⁻⁴³
(dσ/dQ²dQ₃)SYM (cm²/GeV⁴)
0
1
2
3
4
5
6
7
8
Q₃ (GeV)
1873C10

Fig. 10

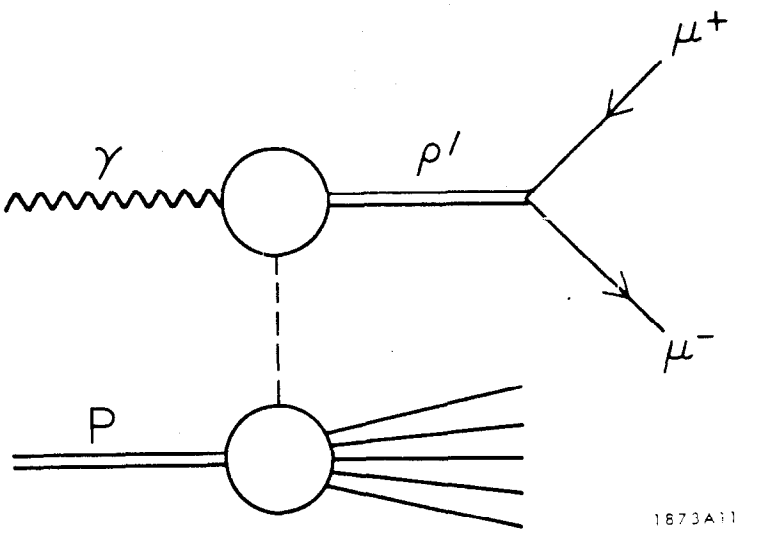

Fig. 11

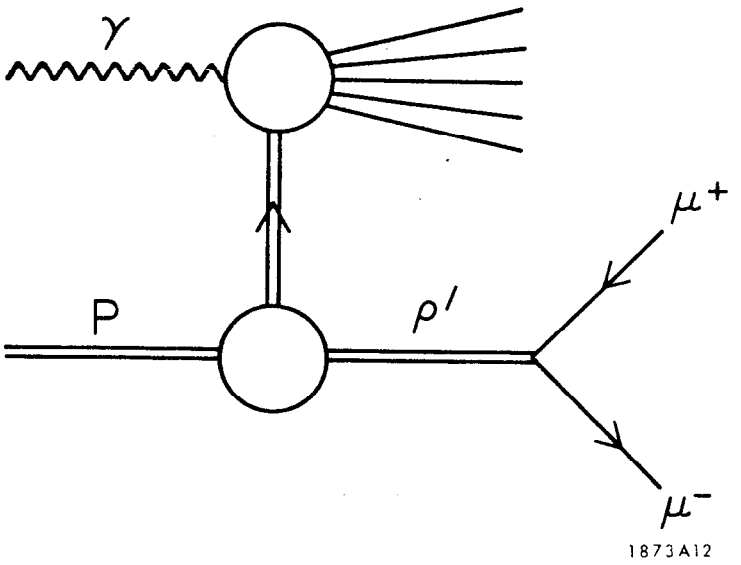

Fig. 12

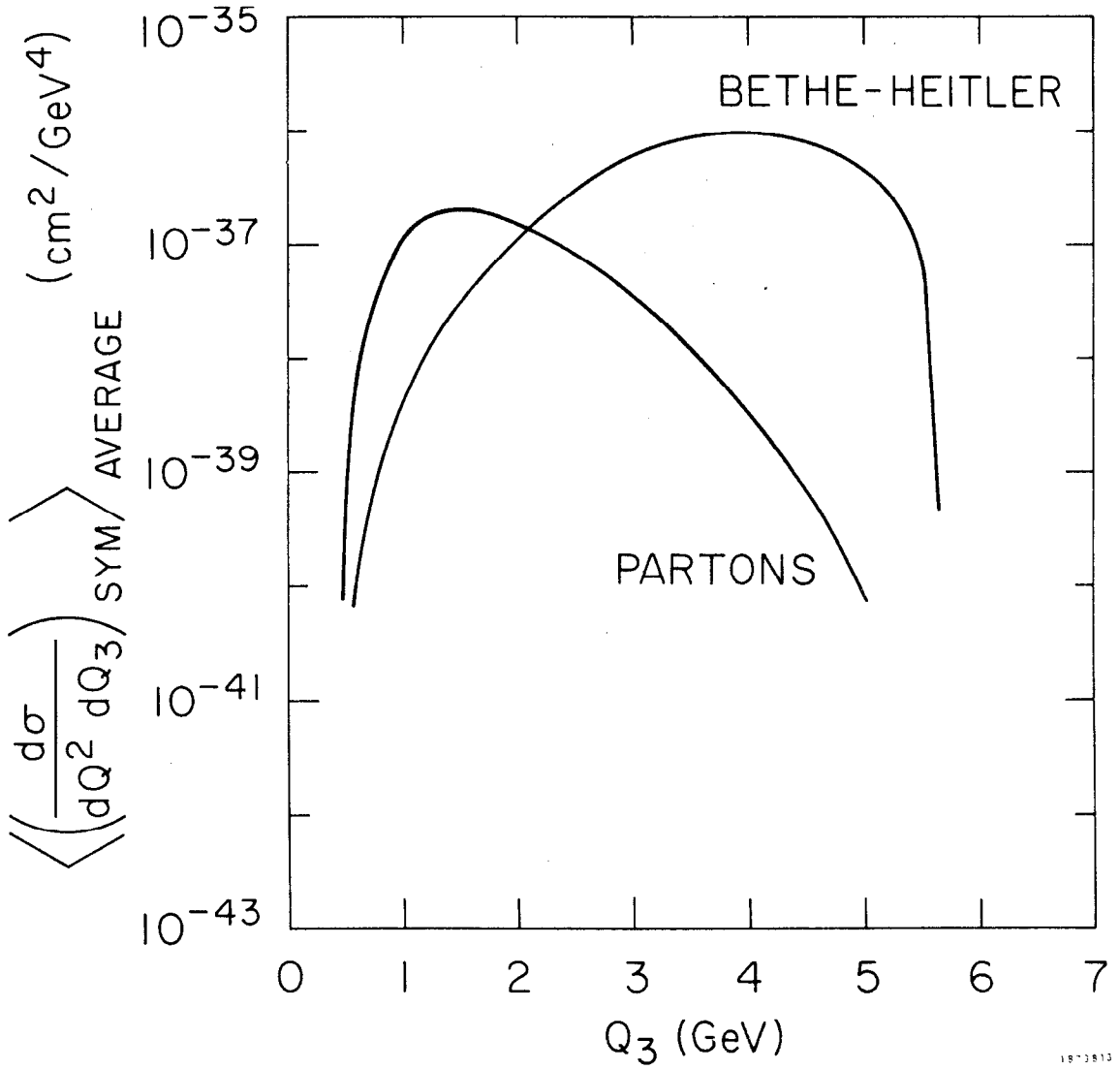
BETHE-HEITLER
PARTONS
10^{-35}
10^{-37}
10^{-39}
10^{-41}
10^{-43}
0
1
2
3
4
5
6
7
Q_3 (GeV)
$\left\langle \left(\frac{d\sigma}{dQ^2\, dQ_3} \right)_{SYM} \right\rangle$ AVERAGE (cm^2/GeV^4)

Fig. 13